8 Theoretical Description of Rare-Gas Clusters Under Intense Laser Pulses

Ionuţ Georgescu[1], Ulf Saalmann[1], Christian Siedschlag[2], and Jan M. Rost[1]

[1] Max Planck Institute for the Physics of Complex Systems · Nöthnitzer Str. 38, 01187 Dresden, Germany
e-mail: us@pks.mpg.de, rost@pks.mpg.de
[2] FOM Institute for Atomic and Molecular Physics, Kruislaan 407, 1098 SJ Amsterdam · The Netherlands

Summary. We discuss the ionization and explosion dynamics of rare-gas clusters under intense femtosecond laser pulses. On one hand, we show how a microscopic treatment by means of a mixed quantum/classical approach provides detailed and time-resolved insight into the mechanisms of excitation and ionization of the irradiated clusters. Furthermore, we compare the cluster response to standard 780 nm light pulses with the response to 100 nm pulses, already obtained at an VUV-FEL source, and with 3 nm light, which will be available from future XFEL sources. On the other hand, we present a simple analytical model which idealizes the single-cluster dynamics but considers the real experimental scenario, i.e., a laser beam profile and a cluster size distribution. Only thereby one can achieve agreement with experimental data on a quantitative level as demonstrated for the kinetic energy distribution of the ionic fragments.

8.1 Introduction

Clusters absorb light very efficiently which becomes clear from the phenomena observed, like the production of highly charged ions [1, 2], energetic electrons and ions [3–5], X-rays [6, 7], or neutrons [8–11]. A more exhaustive list of references, also to theoretical work, can be found in a recent review [12]. The efficient energy absorption is rooted in the nature of clusters: between the condensed and the gas phase, a cluster is much denser than a gas, thus absorbing more energy than isolated particles. Yet, it does not have as many dissipation channels, e.g., lattice vibrations, as a solid.

A number of experiments have additionally revealed that an optimum pulse length T_{crit} exists for maximum energy absorption, where T_{crit} changes substantially under different conditions, such as the kind of cluster atoms, the size of the cluster and the peak intensity of the laser pulse [13–18]. Here, we will give a brief review over energy absorption mechanisms with particular emphasis on the conditions for optimum absorption. Under this aspect we will also briefly discuss the first results at 100 nm wavelength and set the stage for light with even another order of magnitude shorter wavelength, namely 3 nm. These new parameter regimes of light-matter interaction will become accessible with the advent of intense VUV and XUV pulses from free-

electron laser sources [19]. To quantify the different regimes we present in Table 8.1 the response of free electrons to lasers of various wavelengths λ and intensities I in terms of the quiver amplitude (i.e. the excursion length) $x_{\text{quiv}} := \sqrt{I}\lambda^2/c^2$ and the ponderomotive energy (i.e. the mean kinetic energy) $E_{\text{pond}} := I\lambda^2/4c^2$. We will later refer to the values shown in this table.

Common to all clusters subjected to strong laser pulses of different wavelength is the three-step scenario sketched in Fig. 8.1. In a first phase (termed I), the light couples to the atoms as if they were isolated, the cluster environment does not have an effect. In phase II, the critical and interesting phase, the cluster expands due to the ions created in phase I leading to a decreasing density of ions. On the other hand, the density of so called "quasi-free" electrons in the cluster does not necessarily decrease. These electrons are said to be "inner-ionized" but not yet "outer-ionized", i.e., they are still bound to the cluster but no longer to a specific ion. The net change of

Table 8.1. Ponderomotive energies E_{pond} and quiver amplitudes x_{quiv} for long and short laser wavelengths λ at different intensities I

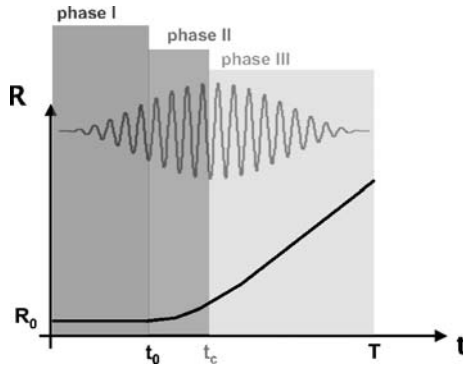| wavelength		intensity I		
		$10^{14}\,\text{W/cm}^2$	$10^{16}\,\text{W/cm}^2$	$10^{18}\,\text{W/cm}^2$
$\lambda = 780\,\text{nm}$	E_{pond}	$5.67\,\text{eV}$	$567\,\text{eV}$	$56.7\,\text{keV}$
	x_{quiv}	8.28Å	$82.8\,\text{Å}$	$828\,\text{Å}$
$\lambda = 100\,\text{nm}$	E_{pond}	$93\,\text{meV}$	$9.3\,\text{eV}$	$932\,\text{eV}$
	x_{quiv}	$0.136\,\text{Å}$	$1.36\,\text{Å}$	$13.6\,\text{Å}$
$\lambda = 3.5\,\text{nm}$	E_{pond}	$0.1\,\text{meV}$	$0.01\,\text{eV}$	$1.1\,\text{eV}$
	x_{quiv}	$0.0002\,\text{Å}$	$0.002\,\text{Å}$	$0.02\,\text{Å}$

Fig. 8.1. Typical cluster dynamics under a strong laser pulse in terms of the time dependent cluster radius $R(t)$. Atomic ionization (phase I), critical expansion (II) and relaxation (III), see text. The laser pulse is also indicated

their density depends on the balance of inner and outer ionization at each instant of time. Finally, during phase III energy is redistributed within the cluster, e.g., through recombination. The cluster completely disintegrates and the final (measurable) distribution of ions and electrons is built up. This relatively simple yet quite universal scheme facilitates the understanding and assessment of the very different mechanisms of energy absorption we will discuss. Concerning the theoretical description we will restrict ourselves to the approach we have followed, namely a classical molecular dynamics simulation of the cluster explosion where the coupling of the bound electrons to the laser light and/or existing electric fields is described by quantum rates. This is to date the only approach which permits to reach relatively large clusters without additional approximations and has been developed by a number of authors [20–31].

8.2 Quasi-classical Microscopic Description

The key idea [22] which has proven to provide physical insight and numerical efficiency is the division of the ionization process into *inner* and *outer* ionization[3]. Here, inner ionization means energy absorption of bound electrons resulting in so-called quasi-free electrons. They are not bound anymore to a particular atom but still to the cluster as a whole, which can provide a sufficiently strong space charge to hold the electrons back. Eventually, quasi-free electrons may be further heated until they are ejected into the continuum, which we call outer ionization.

The dynamics of bound electrons with typical oscillation periods of a few attoseconds are not treated explicitly. Rather one uses a statistical approach to describe it by means of the occupation number of bound levels which may change after each time step. The probability for a particular transition within a time step is calculated as the product of the corresponding rate Γ and the time step Δt. This probability $p = \Gamma \cdot \Delta t$ is compared to a random number ξ distributed uniformly in the interval [0,1]. A transition takes place if $p > \xi$. The rates Γ may crucially depend on the laser (intensity and frequency) and the current state of ion, see the following sections 8.2.1 to 8.2.3. For clusters, the Coulomb field of the neighboring ions and electrons has to be taken into account for a proper description of the inner-ionization process.

An inner-ionization event "gives birth" to a quasi-free electron, which is subsequently propagated classically along with the ions and other quasi-free electrons with all mutual Coulomb forces included. This propagation

---

[3] In a strict sense this is only possible in rare-gas clusters. However, the delocalized valence electrons of metallic clusters should be of minor importance for the creation of the high charge states observed, since these electrons are emitted early in the pulse.

accounts for electron–electron and electron–ion scattering which is important because of the high particle density in the cluster volume. Furthermore, for infrared/visible and VUV frequencies the laser may additionally heat these quasi-free electrons.

8.2.1 Inner Ionization in Low-Frequency Fields

In low-frequency laser pulses, the inner ionization occurs from top to bottom, i.e., the most weakly bound electron is ionized with the highest probability. For sufficiently high fields the ionization of an electron with the binding energy E_{ip} to an ion of charge q is due to barrier suppression (above-the-barrier ionization). For weaker fields the electron can still leave the ion by tunneling through the barrier. The tunneling probability may be obtained [24] from the ADK formula [32]. Since the formula is derived for a homogenous electric field one should be careful for the case of clusters where additional contributions to the electric field from the other particles (electrons and ions) may be important. Therefore, it has been proposed [26] to calculate directly the tunnel integral [33]

$$s = \int_0^1 d\tau \sqrt{V(\boldsymbol{r}_\tau) - E_{ip}} \,, \qquad \boldsymbol{r}_\tau = \boldsymbol{R} + \tau \boldsymbol{X} \qquad (8.1)$$

with the electric total field at the ionic position $\boldsymbol{R}$ pointing in the direction $\boldsymbol{X}$, with $|\boldsymbol{X}| = 1$. The potential V in (8.1) is composed of the laser and all the other particles not just the ion under consideration. The tunnel probability is finally $P = \exp(-2s)$.

8.2.2 Inner Ionization in VUV Fields

Atomic ionization by 100-nm lasers is perturbative below a laser intensity of $\sim 10^{16}\,\text{W/cm}^2$ (see Table 8.1). Hence, calculating the atomic photo*absorption* rates [34] for the respective outermost electron of each cluster atom forms the starting point for inner ionization. With the frequency of 12.7 eV used in the first FEL experiments at DESY [35] one can only singly ionize an isolated xenon atom. In a cluster environment neighboring ions lower the effective threshold for inner ionization given by the effective binding energy $E_{eff} = E_{bar} - E_b$, where E_{bar} is the energy of the closest barrier to the atom or ion out of which the electron is to be ionized, and E_b the energy of the bound electron (taken to be the binding energy of an isolated atom/ion plus the additional potential energy due to the laser field and the surrounding charges). Whenever a photon is absorbed and $\omega > |E_{eff}|$, the outermost electron of the ion is ionized and henceforth treated as a classical particle. This process is, in principle, repeated until all electrons are inner-ionized. In practice, however, it turns out that in almost all cases only the 5s and 5p electrons of xenon are ionized.

8.2.3 Intra-Atomic Processes in High-Frequency Fields

For high-frequency laser impact, the laser-atom interaction is of non-relativistic and perturbative nature, as in the previous case, yet the light acts fundamentally differently on the bound electrons: Ionization starts from the inside because photo-ionization cross sections at X-ray wavelengths are considerably higher for the inner shells than for the valence shells [36]. In first-order perturbation theory cross sections scale as $\sigma \propto E_{\rm b}^{7/2}$ for $\hbar\omega > E_{\rm b}$. Typically, the inverse rates are $1\ldots10\,\mathrm{fs}$ and thus much smaller than the pulse length of about $100\,\mathrm{fs}$. Hence, multiple single-photon ionization is possible, in particular since the inner-shell holes created by photo-ionization are refilled by Auger-like processes. The Auger decay is only weakly dependent on the atomic charge state[4] and occurs fast, typically in $0.2\ldots5\,\mathrm{fs}$ [37]. Due to this almost instantaneous refilling of the inner shells they can be ionized many times during the pulse and the atoms can be "pumped dry" efficiently. The ionization occurs "inside-out" exactly opposite to the mechanism in the visible and VUV-wavelengths regime where the most weakly bound electrons are removed first. The ionization cascade may stop for highly charged ions where the increasing binding energy of the remaining electrons may prevent both, photo- and auto-ionization, for energetical reasons.

Non-dipole effects in the interaction with single atoms/ions do not have any crucial influence apart from distortions of the angular distribution of the photoelectrons [38]. For the interaction with the clusters they are negligible because of the vanishing impact of high-frequency light on quasi-free electrons.

8.2.4 Outer Ionization

The numerical (classical) propagation of the inner-ionized electrons is straight forward apart from two aspects: instability of classical particles and an unfortunate scaling with the particle number. To circumvent the first problem one may introduce a smoothed Coulomb interaction [21]

$$W_{ij}(\boldsymbol{r}_i, \boldsymbol{r}_j) := \frac{q_i\,q_j}{\sqrt{r_{ij}{}^2 + \alpha}} \tag{8.2}$$

for two particles with charge q_i and q_j separated by the distance $r_{ij}{}^2 = (\boldsymbol{r}_i - \boldsymbol{r}_j)^2$. The smoothing parameter α "regularizes" the Coulomb potential and prevents the collapse of ions and electrons. The same effect can be obtained by a short-range repulsive part which additionally accounts for elastic scattering [22]. Furthermore, (8.2) simplifies the numerical integration by avoiding strong gradients for close collisions.

---

[4] For the idealized case of hydrogenic wave functions it can be shown that the matrix element for Auger decay according to Fermi's golden rule is completely independent of the nuclear charge.

Due to the long-range nature of the Coulomb interaction the calculation of the forces on all N particles of the systems scales as N^2. In order to handle clusters with more than $\sim 10^3$ atoms (including the electrons $N \sim 10^4$) one is forced to use special algorithms which take advantage of the long-range interactions between a large number N of particles, e.g., hierarchical tree codes [39]. Originally developed for gravitational N-body problems in cosmology [40], such hierarchical tree codes allow one to follow the dynamics of all charged particles over a few hundred femtoseconds with typical time steps of attoseconds [27, 31].

In the long-wavelength and the VUV regime the laser is coupled to the electrons as a classical field. The quasi-free electrons are driven over distances of the respective quiver amplitudes (see Table 8.1), or experience substantial inverse bremsstrahlung (IBS) heating due to repeated forced collisions with the ions. In the case of high-frequency radiation, the field is oscillating so fast that an electron cannot gain substantial velocity and one can completely neglect the laser field in the classical equations of motion.

Note, that despite the short wavelength the dipole approximation remains valid, since the quiver amplitude is much larger than the wavelength, even for high intensities (see Table 8.1). Furthermore, Compton scattering effects are not taken into account [28] due to their small cross section.

8.3 Dynamical Phenomena and Their Dependence on Laser Wavelength and Cluster Size

8.3.1 Cooperative Behavior in Small Clusters ($\lambda = 780$ nm)

Simulation of the charging in small rare-gas clusters along the lines described in the last section have revealed the existence of an optimum pulse length for maximum charging of the cluster. This optimum pulse length was traced back to an optimum mutual ionic separation R_{ei}, where "ei" stands for enhanced ionization (EI). First discovered for diatomic molecules [41, 42] it applies for small clusters in full analogy [26, 43]. It is characterized by an independence of R_{ei} from the laser frequency (as long as its period is adiabatically slow compared to the orbital times of the electrons). A slightly different expansion speed of the cluster for different laser frequencies leads to a small frequency dependence of the experimentally accessible optimum laser pulse length although the mechanism of EI is operative. In contrast to diatomic molecules EI occurs in clusters also for circularly polarized light [26]. This is easy to understand, since in a (spherical) cluster the rotating polarization vector always finds two ions in a line, which is required for EI. The "simplest" way to proof EI experimentally would be to use a laser with a frequency which is higher than the plasmon frequency of the unperturbed cluster. Then resonant absorption (see next section) cannot occur and EI could be clearly attributed to the mechanism of EI.

EI is by no ways a collective behavior, it is rather the *cooperative effect* of two ions in line (there are a few of these pairs in a cluster) with the instant polarization vector which helps to outer-ionize the electron. Clearly, it does not work if there is another shell of ions beyond the outer ion which prevent outer ionization. Hence, EI is limited to small clusters. However, the number of atoms of the cluster is not the only limiting factor. Another one is the number of quasi-free electrons generated during the pulse, i.e., those electrons, which are inner-ionized, but not immediately outer ionized. These quasi-free electrons may absorb (possibly collectively) energy from the laser pulse, a mechanism which we will discuss next.

8.3.2 Collective Behavior in Medium Sized Clusters ($\lambda = 780$ nm)

The collective behavior emerges from the possibility to match an internal frequency of the cluster, namely that of the center-of-mass (CM) motion of the quasi-free electrons Ω, with the external driving frequency ω of the laser.

In general, considering typical electron densities in the cluster, this frequency is much too high. However, when the cluster expands, the density decreases, and in turn also the eigenfrequency of the quasi-free electrons,

$$\Omega(Q, R) = \sqrt{Q/R^3} \ . \tag{8.3}$$

The usual picture, from which this quantitative relation is deduced, starts with two spheres of constant but opposite charge density which are shifted with respect to each other along a line out of the force free equilibrium through the external force (in our case the dipole coupling to the laser field). As a consequence a restoring harmonic force is generated whose force constant Ω provides the eigenfrequency of the collectively excited system of electrons and ions. This excitation is identical to a surface plasma excitation[5] of a confined electron plasma. Since the density is a function of the cluster radius, the frequency is also directly a function of the cluster radius, and the resonance condition

$$\Omega(Q, R_{\mathrm{ra}}) = \omega \tag{8.4}$$

leads, as in the case of enhanced ionization, to a critical cluster radius R_{ra}, where "ra" stands for resonant absorption. However, there are striking differences. Quantitatively, the relation $R_0 < R_{\mathrm{ei}} < R_{\mathrm{ra}}$ holds, i.e., the radius for enhanced ionization R_{ei} is smaller than that for resonance absorption R_{ra} but larger than the equilibrium radius R_0. This has been revealed clearly in [45] where both mechanisms, enhanced ionization and resonance absorption, could

---

[5] The eigenfrequency can be written in terms of the charge density ρ_{ion} (assumed to be homogeneous) as $\Omega = \sqrt{4\pi\rho_{\mathrm{ion}}/3}$. For a neutral system with $\rho_{\mathrm{ion}} = \rho_{\mathrm{quasi}} = \rho$ it reads $\Omega = \sqrt{4\pi\rho/3} = \omega_{\mathrm{pl}}/\sqrt{3}$ with ω_{pl} the plasma frequency. This is the classical surface plasmon frequency of a spherical cluster [44].

be identified in a single cluster expansion. Secondly, collective excitation is strongly frequency dependent in contrast to enhanced ionization.

Resonance absorption (RA) occurs also in metal clusters for the valence electrons. This requires of course laser fields which must not be so strong that the loosely bound valence electrons are lost immediately by field ionization, typical intensities are up to 10^{12} W/cm^2 [46,47]. Even small clusters exhibit RA if the number of quasi-free electrons is large enough, see the Platinum cluster experiment [13] or more recent experiments with silver clusters [18].

Surprisingly, the entire CM electron dynamics of the cluster can be described as the solution $X(t) = A_t \cos(\omega t - \phi_t)$ to a driven damped oscillator with the equation of motion [27]

$$\ddot{X}(t) + 2\Gamma_t \dot{X}(t) + \Omega_t^2 X(t) = F_0(t) \cos(\omega t) . \tag{8.5}$$

The amplitude A_t, phase ϕ_t, damping Γ_t, and eigenfrequency Ω_t are quasi-stationary variables whose change in time, indicated by the index t, is much slower than the laser period $2\pi/\omega$. The four variables are not independent, one can express Γ_t and Ω_t in terms of A_t and ϕ_t,

$$\Omega_t^2 = \omega^2 + F_0/A_t \cos \phi_t , \qquad \Gamma_t = F_0/(2A_t\omega) \sin \phi_t . \tag{8.6}$$

This allows us to extract the eigenfrequency and damping from the CM-velocity, provided it really obeys the dynamics $X(t)$ of a driven damped harmonic oscillator. The result, along with the determination of the eigenfrequency directly from the density of ions in the expanding cluster, is shown in Fig. 8.2. One sees that the damping reaches its maximum with $\Omega \approx \Gamma$ at resonance which is in the framework of (8.5) a direct consequence of a roughly constant amplitude A.

This holds also true for clusters which contain an order of magnitude more atoms, i. e. 10^4 instead of 10^3 [31]. The strong change in (negative) slope of the lower bright trace in the electron energy spectrum at $t = -300$ fs in Fig. 8.3 is due to a sudden increase of positive background charge which indicates increased outer ionization. The reason is efficient energy absorption since the resonance condition is met as the phase lag of $\pi/2$ between the driving laser field and the electron CM motion shows (inset of Fig. 8.3). However, the laser pulse must be long enough so that the cluster can expand until the resonance condition at low enough electron density is met during the pulse.

8.3.3 Nonlinear Behavior in Large Clusters ($\lambda = 780$ nm)

If the conditions are suitable, than RA is also for large clusters (with more than 10^4 atoms) the most efficient mechanism, simply because it includes the majority of the available electrons. This was already realized by Ditmire and coworkers who introduced the nano-plasma model [48]. It is the linear macroscopic equivalent to RA as described in the last section. Derived within a hydrodynamic approach it extends the mechanism of RA to very large clusters.
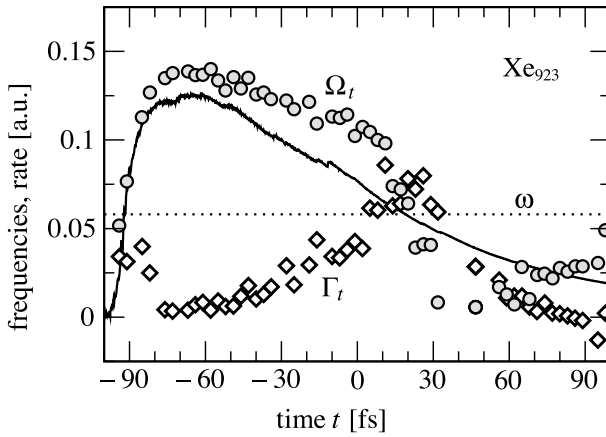
Fig. 8.2. Parameters of the harmonic oscillator model (8.5) as calculated from the Xe$_{923}$ dynamics. Shown are the eigenfrequency Ω_t according to (8.3) as *solid line* and from (8.6) with *circles*, as well as the damping rate Γ_t from (8.6) with *diamonds* and the laser frequency (*dotted line*). Graph from [27]
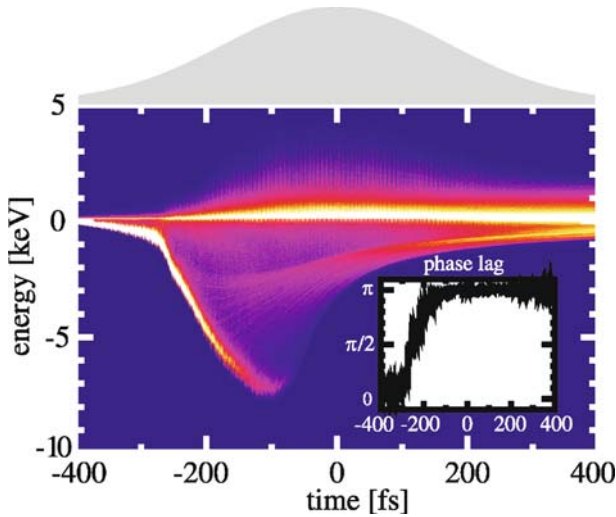

Fig. 8.3. Time resolved energy spectrum of cluster electrons under a laser pulse of the form $F(t) = \exp(-\log 2(2t/T)^2)\cos\omega t$ with half width (pulse length) $T = 400$ fs (the laser pulse envelope is indicated in grey above the contour plot) for a cluster of 9093 xenon atoms. Bright color corresponds to large number of electrons having the corresponding energy at the respective time. The inset shows the phase lag ϕ_t of the electronic CM motion

However, often it lasts longer than the pulse length before a large cluster has expanded sufficiently to reach the resonance condition (8.4). Hence for large clusters other less effective absorption mechanisms become relevant under laser pulses with a length of the order of 100 fs. Since these mechanisms typically involve only a small number of electrons with properties which uniquely characterize the effect, these mechanisms are much harder to identify and to confirm experimentally. We only mention here a number of interesting ideas. They all have in common that they provide means to disrupt the harmonic quiver motion of electrons with the consequence of a phase difference and resulting energy absorption. Inhomogeneous fields in the cluster, including edge effects, can play a major role as argued in different ways [49–51]. Phase disrupting back-scattering in fair analogy to the Fermi-shuttle mechanism has been discussed [7].

8.3.4 Efficient Inverse Bremsstrahlung for a Strongly Inner-Ionized Cluster in VUV Light ($\lambda = 100\,\mathrm{nm}$)

The first (cluster) experiments at the free electron laser of DESY with laser pulses of $\sim 10^{14}$ W/cm^2 peak intensity, 50–100 fs duration and a wavelength corresponding to 12.7 eV photon energy have opened a completely new regime of matter–light coupling [35, 52–54]. The concepts from 780 nm light pulses were not suitable to understand the experimental results. While the photon frequency suggests inverse Bremsstrahlung (IBS) as the dominant absorption mechanism, the experimentally determined number of absorbed photons (about 50 photons per cluster atom) was much to high to be explained by standard IBS given the observed ionic charges (about 2 photons per atom according to simple model calculations [35]). Moreover, the average degree of ionization (for a cluster with roughly 80 xenon atoms, e.g., 1.5 fold) was significantly smaller than the highest charges observed (up to 6 fold charged xenon). The latter effect points to the built-up of charge inhomogeneities. This is indeed the case [29] and it is only possible in the absence of quiver motion (which is negligible here, cf. Table 8.1) while it wipes out all possible charge imbalances in distributions for small clusters under 780 nm light.

The high efficiency of energy absorption prompted the introduction of a model [55] with a modified atomic potential were quasi-free electrons in the cluster would "see" a higher ionic charge than the charge of a cluster ion suggested. However, a microscopic calculation along the principles as discussed in Sect. 8.2 revealed that standard IBS can explain the efficient energy absorption as well, considering that many more electrons are subjected to heating by IBS. These electrons are created by single photo ionization of xenon ions *into* the cluster due to a significant lowering of the barriers between neighboring ions. This is like a ladder-ionization, where the 12.7 eV photon energy is always sufficient to ionize the least bound electron of an ion into the cluster. The quasi-free electrons cannot easily leave the cluster, due
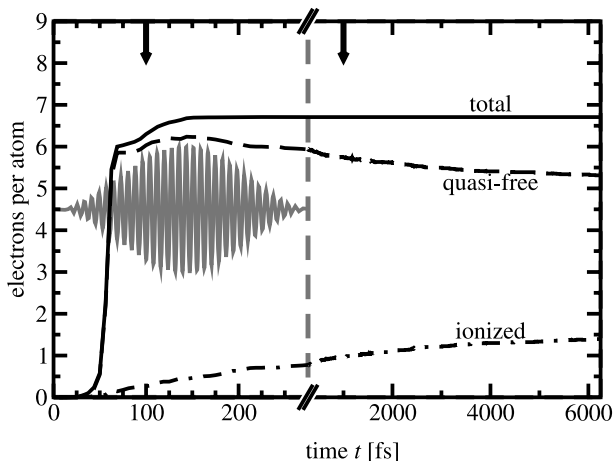
Fig. 8.4. Number of electrons as a function of time in an Xe_{147} cluster irradiated by a 90 nm laser pulse (indicated by the *gray curve*). We show quasi-free (*dashed line*) and free (*dot-dashed line*) electrons as well as the sum of both (*solid line*). Note the different time scales for $t < 275$ fs and $t > 275$ fs, respectively. (For the *arrows* see Fig. 8.5)

to the large background charge of the ions which has been built up which results in a relatively large number of quasi-free electrons compared to the much fewer ionized electrons, see Fig. 8.4. From the figure one also notes that, in contrast to infrared laser pulses, the ionization continues until long after the pulse is over. In fact, the quasi-free electrons form a nano-plasma for clusters as small as 100 atoms and the thermalized quasi-free electrons obey a Maxwellian velocity distribution (Fig. 8.5) whose high velocity tail supplies the ionizing electrons which slowly "boil off" the cluster even after the pulse is over.

At times later than shown in Fig. 8.4, many of the quasi-free electrons will recombine, leading to the finally observed spectrum of charges. Hence, the transient average charge of the ions is much higher than concluded from the finally observed ion spectrum and the efficient energy absorption can be explained by standard IBS [29], which yields for Xe_{147} about 35 absorbed photons per atom. A similar conclusion was reached in [30], where, however, the inner-ionization and recombination processes in the cluster were interpreted differently.

The recombined electrons have higher average energy than the quasi-free electrons and do not thermalize any more (light gray shaded region in the right panel of Fig. 8.5). Consequently, they have to be discarded when fitting a Maxwellian shape to the velocity distribution of inner-ionized electrons (dark grey shaded region in the right panel of Fig. 8.5).
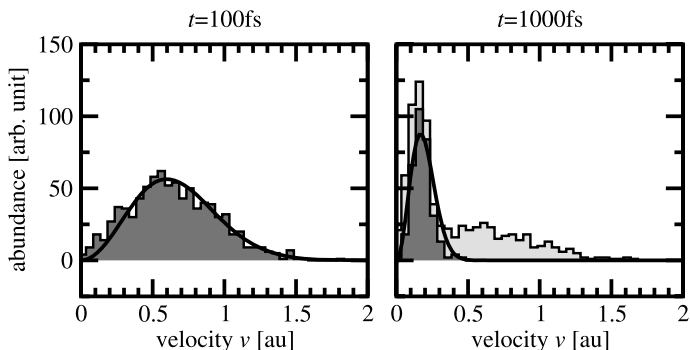
Fig. 8.5. Velocity distributions of the electrons at two times (marked by vertical arrows in Fig. 8.4): at $t = 100$ fs during the pulse and before cluster expansion (*left panel*) and at $t = 1000$ fs after the pulse (*right*). For the later time we show distribution for all electrons in the cluster volume (*light gray*) and for the case when the recombined electrons are excluded (*dark gray*); for the earlier time both distribution coincide. Additionally, we show fits to a Maxwell distributions (*solid lines*)

8.3.5 Hollow Clusters Formed Under 3.5 nm Laser Pulses

To illustrate the wealth of phenomena in laser-cluster interaction we discuss now laser pulses whose wavelength is roughly a factor 100 shorter than in the VUV light in the last section. Clearly, even with extremely high intensity, light with this frequency acts perturbatively on the electrons (Table 8.1). In fact, apart from single photo-ionization or excitation of bound electrons, there is no effect of the laser pulse so that the dynamical evolution is only due to the forces between charged particles of the cluster. The dynamics of clusters in strong short-wavelength X-ray laser pulses is much less studied and understood than the one of clusters exposed to pulses of longer wavelengths. The main reason is the lack of experimental data. Such data will be available only if the planned XFEL machines [19] at DESY in Hamburg [56], at the LCLS in Stanford [57], or at BESSY in Berlin [58] will start operating in the next years.

The first theoretical studies concentrate on the ionization and fragmentation dynamics of various cluster types [28,59–61]. This is of crucial importance for the planned imaging investigations with XFEL machines: On one hand the extreme brilliance of the XFEL helps to get sufficient intensity in the diffraction pattern of a sample in the beam. On the other hand, however, this beam strongly ionizes the sample which will therefore undergo fragmentation. The key question is on which time scale compared to the laser pulse this "loss of structure" occurs. Atomic clusters will be among the first targets in strong X-ray beams to address this question experimentally. Hence, one needs to understand the basic ionization mechanism for these systems. Our first studies with small Argon clusters have concentrated on the electron dynamics at

a photon energy of $\hbar\omega = 350\,\text{eV}$ which is only slightly larger than the binding energy of the L-shell of Argon. This permits insight into the importance of competing excitation/ionization processes. In other studies [28,62] the laser frequency was chosen equal to the highest one available in the near future. Main emphasis was put on the question whether X-ray imaging will be possible or not when the atoms are stripped of their electrons and move due to their Coulomb repulsion.

Figure 8.6 shows the final charge per atom of two different clusters at $\hbar\omega = 350$ eVas a (measurable) indicator for the energy absorption. As an overall feature, we note lower final charges for the cluster atom compared to the isolated atom (where just the rate equations according to Sect. 8.2.3 have been solved), a difference which increases with the size of the cluster. This indicates a considerable influence of the cluster environment on the photo-ionization process with the result that clusters are less effectively ionized at high fields than atoms.

The first reason for the reduced final charge of the cluster is the space charge. It suppresses outer ionization since the electrons have only gained the difference between the photon energy and the binding energy relative to the other cluster ions which is not enough to overcome the space charge. Secondly, the rapidly oscillating laser field cannot drive quasi-free electrons against the positive space charge out of the cluster which is evident from the small quiver amplitudes listed in Table 8.1.

However, there is another, less obvious, reason for the reduced energy absorption due to the cluster environment. The inner-shell holes created by photo-ionization will decay by subsequent ionization processes like auto-ionization or shake-off processes. At a first glance one would expect that such intra-atomic processes are not affected by the cluster environment. However, the strong laser impact creates local charges in the cluster which deform weakly-bound electronic states and even delocalize electrons since the Coulomb barriers to neighboring ions are lowered. Hence valence electrons are "turned" into quasi-free electrons which screen local charges. The delocalization of the valence orbitals quenches the Auger decay rates because the overlap with the (localized) core holes becomes smaller. As a consequence, the inner shells to be ionized are no longer efficiently refilled by inter-atomic decay, i.e. the atoms in the cluster are temporarily hollow. In order to assess the relative importance of the screening effect compared to the suppression of ionization due to the cluster space charge one can artificially exclude tunneling of electrons to neighboring ions which keeps the electrons localized thereby increasing their ionization rates. Note that this applies to primary photo-ionization and secondary auto-ionization processes as well. The result is indicated in Fig. 8.6 where the difference with and without tunneling is marked by grey shading and accounts for the delocalization effect. The remaining difference between the restricted cluster calculation (the dash-dotted line in Fig. 8.6) and that for the atom reveals the space charge effect. For
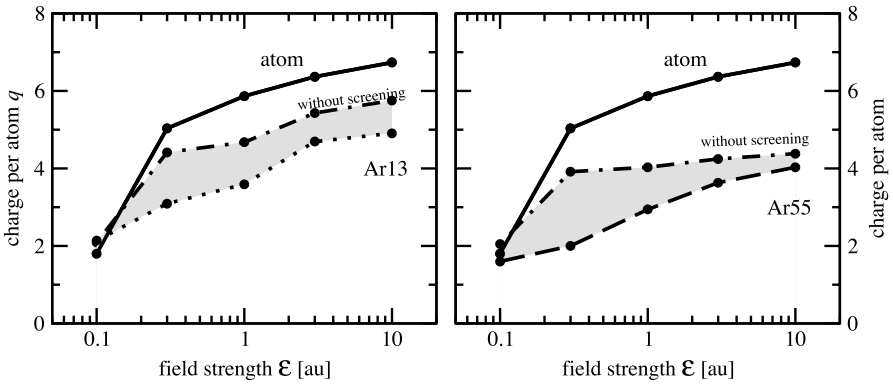
Fig. 8.6. Average charge per atom for two cluster sizes Ar_{13} and Ar_{55} produced by an XFEL pulse ($\hbar\omega = 350\,\text{eV}$, $T = 100\,\text{fs}$) as a function of the field strength $\mathcal{E}$ (*dashed line*). Cluster calculation where intra-cluster screening was precluded (*dot-dashed*) and the isolated atom (*solid*) are shown for comparison. Graph from [59]

field strengths $f \geq 0.3$ au, where differences between atoms and clusters appear, the space charge effect is initially weaker. This changes for stronger fields: Whereas for the smaller cluster Ar_{13} both are of the same magnitude at $\mathcal{E} = 10$ au, for the larger cluster Ar_{55} the space charge effect dominates at this field strength.

The reduced energy absorption of clusters compared to isolated atoms at high frequencies may have important implications for the possibilities to image structures with X-ray pulses: The damage threshold is higher than expected based on isolated atom data and therefore, a cluster or another large structure may sustain a higher photon flux than anticipated. If this also reduces the imaging signal by the same amount must be assessed by detailed calculations in the future.

8.4 Comparison of Theory and Experiment for Cluster Observables Beyond a Qualitative Level

Theoretical considerations in strong field physics often take the laser simply as a spatially homogenous and temporally constant source with intensity I_0. Since the spatial and temporal variation of the laser parameters are usually adiabatic compared to electronic degrees of freedom, one can simply average the calculation for fixed I_0 over the spatial and temporal laser beam profile. This holds in general true also for clusters. However, an additional complication arises from the fact that under experimental conditions clusters have not a unique size with N atoms, but rather a distribution $g(N)$ where the mean N_0 depends on the way they have been generated.

The kinetic energy distribution of the ions (KEDI), e.g., differs substantially for a single cluster under a spatially homogenous laser beam (the theoretical standard) from the experimentally observed KEDI [63]. If we start for simplicity with a homogenous charge distribution of ions in the cluster then three simple steps are sufficient to convert the single cluster KEDI (Fig. 8.7A) to the realistic one, namely averaging over the spatial laser profile (Fig. 8.7B), averaging over the cluster size distribution (Fig. 8.7C), and taking into account saturation in the ionization (Fig. 8.7E).

The basic mechanism underlying the KEDI in clusters is their Coulomb explosion. It converts the potential energy $E_{\mathrm{coul}}(r)$ of a (partially) ionized cluster atom at a distance r from the cluster center into kinetic energy E. The probability $\mathrm{d}P/\mathrm{d}r$ to find an atom at a distance r from the center of the cluster with a homogeneous atomic density is $\mathrm{d}P/\mathrm{d}r = 3r^2 R^{-3}\Theta(R-r)$, where R is the cluster radius. If the cluster is charged homogeneously by the laser pulse with charge q per ion and the ions have not moved yet, then the potential (Coulomb) energy of an ion at radius $r \leq R$ inside the cluster consisting of N atoms is given by

$$E_{\mathrm{coul}}(r, q, N) = Nq^2 r^2/R^3 \ . \tag{8.7}$$

The ions at the cluster edge R have the maximum energy, which sets the energy scale $E_R := E_{\mathrm{coul}}(R, q, N) = q^2 N/R$. Since the Coulomb explosion converts the entire potential energy E_{coul} into kinetic energy E, combining $\mathrm{d}P/\mathrm{d}r$ with (8.7) and defining $\varepsilon = E/E_R$ gives directly the KEDI [64,65],

$$\frac{\mathrm{d}P}{\mathrm{d}\varepsilon} = \frac{3}{2}\sqrt{\varepsilon}\,\Theta(1-\varepsilon) \ , \tag{8.8}$$

which is shown in Fig. 8.7A.

The spatial profile of the laser pulse can be usually described by a Gaussian function with field amplitude $F(\rho) = F_0 \exp(-\rho^2/2\xi^2)$, where ρ is the distance (radius) from the laser beam center in the plane perpendicular to the beam. Along the laser beam we assume a constant intensity since the experiments discussed later [66] are performed with a narrow cluster beam, i.e. a radius smaller than the Rayleigh length [67] of the laser beam. This does not hold for the experiments where the cluster beam is irradiated near the output of the gas-jet nozzle [68].

The charging of the cluster is assumed to be proportional to the field strength, $q \propto F$. This applies for resonant charging of the cluster [27, 31]. Hence, we obtain the spatial distribution of charge $q(\rho)$ by replacing $F(\rho)$ with $q(\rho)$ and F_0 with q_0, the maximum charge per ion reached in the laser focus $\rho = 0$. After integration over ρ the laser profile averaged KEDI reads in terms of the scaled energy $\varepsilon = E/E_{\mathrm{coul}}(R, q_0, N)$

$$\frac{\mathrm{d}P_{\mathrm{las}}}{\mathrm{d}\varepsilon} = \frac{\pi\xi^2 N}{2}\frac{1-\varepsilon^{3/2}}{\varepsilon}\,\Theta(1-\varepsilon) \ , \tag{8.9}$$
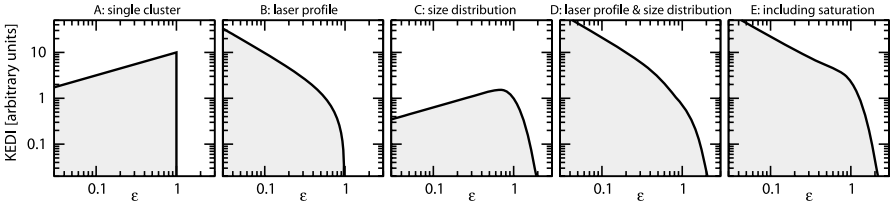
Fig. 8.7. Kinetic energy distributions of ions (KEDI) for Coulomb exploding clusters as function of scaled energy ε, see text. A: single clusters, see (8.8), B: convoluted with a Gaussian laser profile, see (8.9), C: convoluted with a log-normal cluster size distribution, see (8.11), D: effect of laser profile and cluster size distribution combined, see (8.12), E: including saturation of ionization in addition, see (8.14). Graph from [63]

as shown in Fig. 8.7B. What has changed compared to the original KEDI from (8.8) is the qualitatively different behavior with ε^{-1} instead of $\varepsilon^{1/2}$ for small ε. The formal divergence of (8.9) for $\varepsilon \to 0$ can be cured at the expense of a more complicated expression by taking into account that beyond a maximum radius $\rho_{\max}$ the laser intensity is too weak to ionize.

The enhancement of small kinetic energies after averaging over the laser profile is easily understandable from the higher weight of laser intensities less than the peak intensity, which leads to less charging and, consequently, to more ions with smaller kinetic energy.

In most experiments the laser beam interacts with clusters of different size N, which are log-normally distributed [69, 70] according to

$$g(N) = \frac{1}{\sqrt{2\pi}\nu N} \exp\left(-\frac{\ln^2(N/N_0)}{2\nu^2}\right) \ . \tag{8.10}$$

Convoluting the single-cluster KEDI from (8.8) with $g(N)$ yields in scaled units $\varepsilon = E/E_{\mathrm{coul}}(R, q, N_0)$

$$\frac{\mathrm{d}P_{\mathrm{size}}}{\mathrm{d}\varepsilon} = \frac{3}{4} N_0 \sqrt{\varepsilon} \, \mathrm{erfc}\left(\frac{3\ln\varepsilon}{2\sqrt{2}\nu}\right) \ . \tag{8.11}$$

This size-averaged KEDI, shown in Fig. 8.7C, reaches with its tail beyond the energy $\varepsilon = 1$, as more as larger the width parameter ν of the cluster size distribution (8.10) is. The fastest fragments are those from the large clusters in the long tail of this distribution. Note, that we have assumed the average charge q per fragment to be independent of the cluster size N.

Of course, for a realistic experimental KEDI one has to take into account both, the spatial profile of the laser beam and the cluster size distribution. This yields, in a similar manner as for the other distributions,

$$\frac{\mathrm{d}P_{\mathrm{both}}}{\mathrm{d}\varepsilon} = \frac{\xi^2 \pi}{4} \frac{N_0}{\varepsilon} \left[\exp(\nu^2/2) \left(1 + \mathrm{erf}\left(\frac{2\nu^2 - 3\ln\varepsilon}{2\sqrt{2}\nu} \right) \right) \right.$$
$$\left. -\varepsilon^{3/2}\mathrm{erfc}\left(\frac{3\ln\varepsilon}{2\sqrt{2}\nu} \right) \right] . \tag{8.12}$$

Here, we have used $\varepsilon = E/E_0$, with the reference energy $E_0 = E_{\mathrm{coul}}(R, q_0, N_0)$ defined as the maximum Coulomb energy of ions from clusters with the median size N_0 [6] at the laser focus (charge q_0). The corresponding distribution is shown in Fig. 8.7D. Since the spatial laser profile modifies the low-energy part and the cluster size distribution the high-energy part of the ion distribution it is possible to gain information from a measured KEDI on both effects separately.

The final phenomenon which must be taken into account to understand an experimental KEDI is saturation, i.e. the fact, that independent of the laser intensity provided, the charging cannot be higher than a certain maximum value q_{sat}, either because the next atomic shell has a much higher ionization potential or because the atoms are completely ionized. We can model the situation by changing our spatial charging function $q(\rho)$ to

$$q(\rho) = \begin{cases} q_{\mathrm{sat}} & \text{for } \rho \le \rho_{\mathrm{sat}} , \\ q_0 \exp(-\rho^2/2\xi^2) & \text{for } \rho > \rho_{\mathrm{sat}} , \end{cases} \tag{8.13}$$

with q_{sat} the maximum charge, which is realized for clusters close to the center of the laser focus with $\rho < \rho_{\mathrm{sat}}$. The saturation can be characterized by the dimensionless quantity $\eta := q_{\mathrm{sat}}/q_0 \in [0,1]$. The radius of saturation in (8.13) is given by $\rho_{\mathrm{sat}} = \xi\sqrt{-2\ln\eta}$. The charging function (8.13) amounts to using the averaging over the spatial profile only for $\rho > \rho_{\mathrm{sat}}$ and suggests to define the energy scale as $\varepsilon = E/E_{\mathrm{sat}}$ with the saturation energy $E_{\mathrm{sat}} = E_{\mathrm{coul}}(R, q_{\mathrm{sat}}, N_0)$. The result is the KEDI

$$\frac{\mathrm{d}P_{\mathrm{sat}}(\eta)}{\mathrm{d}\varepsilon} = \frac{\mathrm{d}P_{\mathrm{both}}}{\mathrm{d}\varepsilon} - \ln\eta \, \frac{\mathrm{d}P_{\mathrm{size}}}{\mathrm{d}\varepsilon} , \tag{8.14}$$

which develops a characteristic hump before $\varepsilon = 1$, as can be seen in Fig. 8.7E.

To illustrate how the presented expressions for KEDI apply we fit them in Fig. 8.8 to experimental data of very different situations. Whereas xenon clusters do not show any noticeable saturation effect ($\eta = 0.8$, upper two graphs in Fig. 8.8), the large gap between the 1st and the 2nd shell of argon is responsible for the hump seen in the KEDI ($\eta = 0.35$, lower left graph in Fig. 8.8). Finally, hydrogen clusters are extreme cases, since only one electron per atom is available ($\eta = 0$, lower right graph in Fig. 8.8).

Of course, the KEDI derived cannot only be used to interpret experimental spectra regarding mean size and saturation of the cluster. Much more they

---

[6] The median size N_0 separates the higher half of the distribution from the lower half. In a log-normal distribution it is different from the average size which is $\exp(\nu^2/2)N_0$.
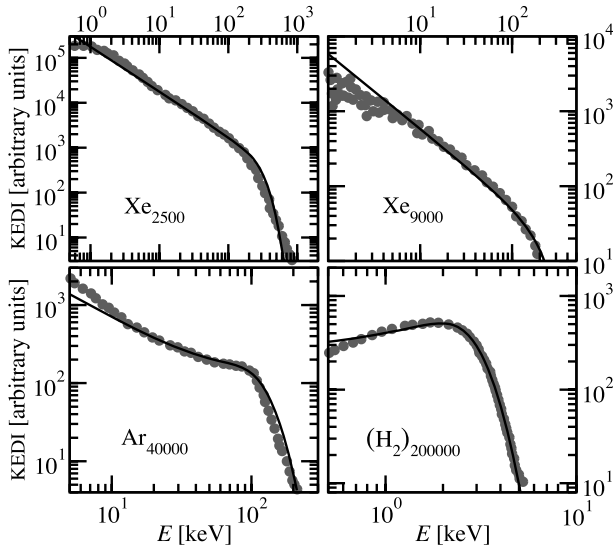
Fig. 8.8. Ion energy spectra for Xe_{2500} [1], Xe_{9000} [71], Ar_{40000} [4] and $(H_2)_{200000}$ [64] clusters from experiments (*circles*) and fits by our model, (8.14) (*solid line*). Graph from [63]

should make it possible to compare single cluster KEDI obtained theoretically via the corresponding convolution to experimental results.

8.5 Summary

Firstly, we have presented a mixed quantum/classical approach: Transitions, according to quantum transition rates, of bound electrons into quasi-free electrons are combined with a classical molecular dynamics for these quasi-free electrons and the created ions. If properly adapted, this approach allows for a microscopic description of laser-cluster interaction for a wide range of laser wavelengths λ, from the infra-red ($\lambda = 780\,\text{nm}$) over the VUV ($\lambda = 100\,\text{nm}$) to the X-ray ($\lambda = 3\,\text{nm}$) regime. The analysis of the, in principle straightforward, propagation showed that the excitation/ionization mechanisms are fundamentally different for the three regimes studied. At $780\,\text{nm}$, where a wealth of experiments has been performed, the dependence of the ionization on the laser pulse length or on the delay in pump-probe measurements, could be traced back to a cooperative behavior of the electrons in small cluster ($\sim 10\,\text{atoms}$) and a collective dynamics in larger clusters ($>100\,\text{atoms}$). Going to $100\,\text{nm}$, with the quiver amplitude about two orders of magnitude smaller, the dominant absorption mechanism seems to be inverse bremsstrahlung. At a even shorter wavelength of about $3\,\text{nm}$, core-level ionization dominates. Surpris-

ingly, this is strongly influenced by the cluster environment in such a way that the ionization of clusters is reduced compared to atoms.

Secondly, we have presented a simple analytical model for the ion kinetic energy spectra of laser irradiated clusters. This model allows one to link quantitatively experimental spectra to typical theoretical single-cluster results. We have been able to fit a number of experimentally available size dependent kinetic energy distribution of the ions, which correspond to the experimental setup in terms of laser profile and cluster distribution we have assumed. We hope, that this link will allow the comparison of observables from cluster experiments with theory on a similar quantitative basis as it is done routinely for atomic or molecular observables.

References

1. T. Ditmire, J. W. G. Tisch, E. Springate, M. B. Mason, N. Hay, R. A. Smith, J. Marangos, and M. H. R. Hutchinson, Nature **386**, 54 (1997)
2. M. Lezius, S. Dobosz, D. Normand, and M. Schmidt, Phys. Rev. Lett. **80**, 261 (1998)
3. Y. L. Shao, T. Ditmire, J. W. G. Tisch, E. Springate, J. P. Marangos, and M. H. R. Hutchinson, Phys. Rev. Lett. **77**, 3343 (1996)
4. V. Kumarappan, M. Krishnamurthy, and D. Mathur, Phys. Rev. Lett. **87**, 085005 (2001)
5. Y. Fukuda, K. Yamakawa, Y. Akahane, M. Aoyama, N. Inoue, H. Ueda, and Y. Kishimoto, Phys. Rev. A **67**, 061201 (R) (2003)
6. A. McPherson, B. D. Thompson, A. B. Borisov, K. Boyer, and C. K. Rhodes, Nature **370**, 631 (1994)
7. C. Deiss, N. Rohringer, J. Burgdörfer, E. Lamour, Ch. Prigent, J.-P. Rozet, and D. Vernhet, Phys. Rev. Lett. **96**, 013203 (2006)
8. T. Ditmire, J. Zweiback, V. P. Yanovsky, T. E. Cowan, G. Hays, and K. B. Wharton, Nature **398**, 489 (1999)
9. J. Zweiback, R. A. Smith, T. E. Cowan, G. Hays, K. B. Wharton, V. P. Yanovsky, and T. Ditmire, Phys. Rev. Lett. **84**, 2634 (2000)
10. G. Grillon, Ph. Balcou, J.-P. Chambaret, D. Hulin, J. Martino, S. Moustaizis, L. Notebaert, M. Pittman, Th. Pussieux, A. Rousse, J-Ph. Rousseau, S. Sebban, O. Sublemontier, and M. Schmidt, Phys. Rev. Lett. **89**, 065005 (2002)
11. K. W. Madison, P. K. Patel, M. Allen, D. Price, R. Fitzpatrick, and T. Ditmire, Phys. Rev. A **70**, 053201 (2004)
12. U. Saalmann, Ch. Siedschlag, and J. M. Rost, J. Phys. B **39**, R 39 (2006)
13. L. Köller, M. Schumacher, J. Köhn, S. Teuber, J. Tiggesbäumker, and K. H. Meiwes-Broer, Phys. Rev. Lett. **82**, 3786 (1999)
14. J. Zweiback, T. Ditmire, and M. D. Perry, Phys. Rev. A **59**, R 3166 (1999)
15. E. Parra, I. Alexeev, J. Fan, K. Y. Kim, S. J. McNaught, and H. M. Milchberg, Phys. Rev. E **62**, R 5931 (2000)
16. V. Kumarappan, M. Krishnamurthy, and D. Mathur, Phys. Rev. A **66**, 033203 (2002)
17. K. Y. Kim, I. Alexeev, E. Parra, and H. M. Milchberg, Phys. Rev. Lett. **90**, 023401 (2003)

18. T. Döppner, Th. Fennel, Th. Diederich, J. Tiggesbäumker, and K. H. Meiwes-Broer, Phys. Rev. Lett. **94**, 013401 (2005)
19. J. Feldhaus, J. Arthur, and J. B. Hastings, J. Phys. B **38**, S 799 (2005)
20. C. Rose-Petruck, K. J. Schafer, K. R. Wilson, and C. P. J. Barty, Phys. Rev. A **55**, 1182 (1997)
21. T. Ditmire, Phys. Rev. A **57**, R 4094 (1998)
22. I. Last and J. Jortner, Phys. Rev. A **60**, 2215 (1999)
23. I. Last and J. Jortner, Phys. Rev. A **62**, 013201 (2000)
24. K. Ishikawa and T. Blenski, Phys. Rev. A **62**, 063204 (2000)
25. E. S. Toma and H. G. Muller, Phys. Rev. A **66**, 013204 (2002)
26. Ch. Siedschlag and J. M. Rost, Phys. Rev. Lett. **89**, 173401 (2002)
27. U. Saalmann and J. M. Rost, Phys. Rev. Lett. **91**, 223401 (2003)
28. Z. Jurek, G. Faigel, and M. Tegze, Eur. Phys. J. D **29**, 217 (2004)
29. Ch. Siedschlag and J. M. Rost, Phys. Rev. Lett. **93**, 043402 (2004)
30. C. Jungreuthmayer, L. Ramunno, J. Zanghellini, and T. Brabec, J. Phys. B **38**, 3029 (2005)
31. U. Saalmann, J. Mod. Opt. **53**, 173 (2006)
32. M. V. Ammosov, N. B. Delone, and V. P. Krainov, Zh. Eksp. Teor. Fiz. **91**, 2008 (1986)
33. L. D. Landau and E. M. Lifschitz, *Quantum Mechanics.* (Pergamon Press, Oxford, 1989)
34. J. M. Rost, J. Phys. B **28**, L 601 (1995)
35. H. Wabnitz, L. Bittner, A. R. B. de Castro, R. Döhrmann, P. Gürtler, T. Laarmann, W. Laasch, J. Schulz, A. Swiderski, K. von Haeften, T. Möller, B. Faatz, A. Fateev, J. Feldhaus, Ch. Gerth, U. Hahn, E. Saldin, E. Schneidmiller, K. Sytchev, K. Tiedtke, R. Treusch, and M. Yurkov, Nature **420**, 482 (2002)
36. M. Ya. Amusia, *Atomic photoeffect.* (Plenum Press New York 1990)
37. A. G. Kochur, V. L. Sukhorukov, A. J. Dudenko, and Ph. V. Demekhin, J. Phys. B **28**, 387 (1995)
38. J. W. Cooper, Phys. Rev. A **47**, 1841 (1993)
39. S. Pfalzner and P. Gibbon, *Many-body tree methods in physics.* (Cambridge University Press, Cambridge, 1996)
40. J. E. Barnes and P. Hut, Nature **324**, 446 (1986)
41. T. Seideman, M. Yu. Ivanov, and P. B. Corkum, Phys. Rev. Lett. **75**, 2819 (1995)
42. T. Zuo and A. D. Bandrauk, Phys. Rev. A **52**, R 2511 (1995)
43. Ch. Siedschlag and J. M. Rost, Phys. Rev. A **67**, 013404 (2003)
44. U. Kreibig and M. Vollmer, *Optical Properties of Metal Clusters.* (Springer Series in Materials Science. Springer, Heidelberg, 1998)
45. T. Martchenko, C. Siedschlag, S. Zamith, H. G. Muller, and M. J. J. Vrakking, Phys. Rev. A **72**, 053202 (2005)
46. F. Calvayrac, P.-G. Reinhard, E. Suraud, and C. A. Ullrich, Phys. Rep. **337**, 493 (2000)
47. T. Fennel, G. F. Bertsch, and K. H. Meiwes-Broer, Eur. Phys. J. D **29**, 367 (2004)
48. T. Ditmire, T. Donnelly, A. M. Rubenchik, R. W. Falcone, and M. D. Perry, Phys. Rev. A **53**, 3379 (1996)
49. T. Taguchi, Jr. T. M. Antonsen, and H. M. Milchberg, Phys. Rev. Lett. **92**, 205003 (2004)

50. C. Jungreuthmayer, M. Geissler, J. Zanghellini, and T. Brabec, Phys. Rev. Lett. **92**, 133401 (2004)
51. S. V. Fomichev, D. F. Zaretsky, D. Bauer, and W. Becker, Phys. Rev. A **71**, 013201 (2005)
52. T. Laarmann, A. R. B. de Castro, P. Gürtler, W. Laasch, J. Schulz, H. Wabnitz, and T. Möller, Phys. Rev. Lett. **92**, 143401 (2004)
53. H. Wabnitz, A. R. B. de Castro, P. Gürtler, T. Laarmann, W. Laasch, J. Schulz, and T. Möller, Phys. Rev. Lett. **94**, 023001 (2005)
54. T. Laarmann, M. Rusek, H. Wabnitz, J. Schulz, A. R. B. de Castro, P. Gürtler, W. Laasch, and T. Möller, Phys. Rev. Lett. **95**, 063402 (2005)
55. R. Santra and C. H. Greene, Phys. Rev. Lett. **91**, 233401 (2003)
56. G. Materlik and T. Tschentscher (eds.) *TESLA Technical Design Report*, vol. V: The X-ray free electron laser (DESY, Hamburg, 2001). see also http://xfel.desy.de
57. J. Arthur, Rev. Sci. Instrum. **73**, 1393 (2002)
    see also http://www-ssrl.slac.stanford.edu/lcls
58. D. Krämer, E. Jaeschke, and W. Eberhardt (eds.) *FEL: Technical Design Report.* (BESSY, Berlin 2004). see also http://www.bessy.de/FEL
59. U. Saalmann and J. M. Rost, Phys. Rev. Lett. **89**, 143401 (2002)
60. U. Saalmann, Interaction of strong X-ray laser pulses with small argon clusters In *Electron and Photon Impact Ionization and Related Topics 2004*, edited by B. Piraux, volume 183 of *Institute of Physics Conference Series*. Institute of Physics Publishing, Bristol and Philadelphia 2004), p. 165
61. M. Bergh, N. Tîmneanu, and D. van der Spoel, Phys. Rev. E **70**, 051904 (2004)
62. Z. Jurek, G. Oszlanyi, and G. Faigel, Europhys. Lett. **65**, 491 (2004)
63. Md. R. Islam, U. Saalmann, and J. M. Rost, Phys. Rev. A **73**, R 041201 (2006)
64. S. Sakabe, S. Shimizu, M. Hashida, F. Sato, T. Tsuyukushi, K. Nishihara, S. Okihara, T. Kagawa, Y. Izawa, K. Imasaki, and T. Iida, Phys. Rev. A **69**, 023203 (2004)
65. J. Zweiback, T. E. Cowan, J. H. Hartley, R. Howell, K. B. Wharton, J. K. Crane, V. P. Yanovsky, G. Hays, R. A. Smith, and T. Ditmire, Phys. Plasmas **9**, 3108 (2002)
66. M. Krishnamurthy, D. Mathur, and V. Kumarappan, Phys. Rev. A **69**, 033202 (2004)
67. A. E. Siegman, *Lasers.* (University Science Books, Sausalito, 1986)
68. M. Hirokane, S. Shimizu, M. Hashida, S. Okada, S. Okihara, F. Sato, T. Iida, and S. Sakabe, Phys. Rev. A **69**, 063201 (2004)
69. J. Gspann, Electronic and atomic impacts on large clusters In S. Datz (ed.), *Physics of Electronic and Atomic Collisions.* (Amsterdam, North-Holland Publishing Company, 1982), pages 79–92
70. M. Lewerenz, B. Schilling, and J. P. Toennies, Chem. Phys. Lett. **206**, 381 (1993)
71. E. Springate, N. Hay, J. W. G. Tisch, M. B. Mason, T. Ditmire, J. P. Marangos, and M. H. R. Hutchinson, Phys. Rev. A **61**, 044101 (2000)